NeuroImage 282 (2023) 120408

Contents lists available at ScienceDirect

NeuroImage

journal homepage: www.elsevier.com/locate/ynimg

Remembering unexpected beauty: Contributions of the ventral striatum to the processing of reward prediction errors regarding the facial attractiveness in face memory

Moe Mihara, Reina Izumika, Takashi Tsukiura *

Department of Cognitive, Behavioral and Health Sciences, Graduate School of Human and Environmental Studies, Kyoto University, Yoshida-Nihonmatsu-Cho Sakyo-ku, Kyoto 606-8501, Japan

ARTICLE INFO

Keywords:
Prediction error
Facial attractiveness
Social reward
Face memory
Hippocampus
fMRI

ABSTRACT

The COVID-19 pandemic has led people to predict facial attractiveness from partially covered faces. Differences in the predicted and observed facial attractiveness (i.e., masked and unmasked faces, respectively) are defined as reward prediction error (RPE) in a social context. Cognitive neuroscience studies have elucidated the neural mechanisms underlying RPE-induced memory improvements in terms of monetary rewards. However, little is known about the mechanisms underlying RPE-induced memory modulation in terms of social rewards. To elucidate this, the present functional magnetic resonance imaging (fMRI) study investigated activity and functional connectivity during face encoding. In encoding trials, participants rated the predicted attractiveness of faces covered except for around the eyes (prediction phase) and then rated the observed attractiveness of these faces without any cover (outcome phase). The difference in ratings between these phases was defined as RPE in facial attractiveness, and RPE was categorized into positive RPE (increased RPE from the prediction to outcome phases), negative RPE (decreased RPE from the prediction to outcome phases), and non-RPE (no difference in RPE between the prediction and outcome phases). During retrieval, participants were presented with individual faces that had been seen and unseen in the encoding trials, and were required to judge whether or not each face had been seen in the encoding trials. Univariate activity in the ventral striatum (VS) exhibited a linear increase with increased RPE in facial attractiveness. In the multivariate pattern analysis (MVPA), activity patterns in the VS and surrounding areas (extended VS) significantly discriminated between positive/negative RPE and non-RPE. In the functional connectivity analysis, significant functional connectivity between the extended VS and the hippocampus was observed most frequently in positive RPE. Memory improvements by face-based RPE could be involved in functional networks between the extended VS (representing RPE) and the hippocampus, and the interaction could be modulated by RPE values in a social context.

1. Introduction

The COVID-19 pandemic has forced people to perceive social signals from faces partially covered by face masks. In such situations, it is common to experience large differences in perceived facial attractiveness between masked and unmasked faces, respectively. As facial attractiveness is processed as a social reward (Tsukiura and Cabeza, 2011b), the difference in the impression of facial attractiveness between masked and unmasked faces reflects reward prediction error (RPE) in a social context. RPE is defined as the difference between predicted and received rewards, and is categorized into positive RPE (increased RPE from the prediction to outcome phases), negative RPE (decreased RPE from the prediction to outcome phases), and non-RPE (no difference in RPE between the prediction and outcome phases). Previous studies have demonstrated that RPE improves episodic memory in the context of monetary rewards (for review, see Ergo et al., 2020). For example, one psychological study reported that the recognition memory of word pairs was significantly enhanced by positive RPE in monetary rewards (De Loof et al., 2018). However, little is known about the neural mechanisms underlying RPE-induced improvement in face memories in the context of social rewards derived from facial attractiveness. To tackle this issue, using event-related functional magnetic resonance imaging (fMRI), we scanned healthy young adult males while they judged the facial attractiveness of masked and unmasked faces during the encoding of

* Corresponding author.
E-mail address: tsukiura.takashi.6c@kyoto-u.ac.jp (T. Tsukiura).

https://doi.org/10.1016/j.neuroimage.2023.120408
Received 10 August 2023; Received in revised form 5 October 2023; Accepted 12 October 2023
Available online 13 October 2023

unfamiliar female faces.

Functional neuroimaging and neurophysiological studies have demonstrated that reward-related regions, including the ventral striatum (VS) and the substantia nigra (SN)/ventral tegmental area (VTA), contribute to the processing of RPE (for review, see Diederen and Fletcher, 2020; Schultz, 2016a; Watabe-Uchida et al., 2017) and that in humans, VS is the most important reward-related region (Garrison et al., 2013; Sescousse et al., 2013). For example, significant activation in the VS has been identified during the processing of RPE for primary rewards (Hare et al., 2008), monetary rewards (Cao et al., 2019) and social rewards derived from facial attractiveness (Bray and O'Doherty, 2007), and linear increases in VS activity as a function of RPE has been found in several fMRI studies (Calderon et al., 2021; Fouragnan et al., 2018; Pine et al., 2018). In addition, there is functional neuroimaging evidence that RPE-related VS activity is shared between monetary and social RPE (Häusler et al., 2015; Lin et al., 2012). These findings suggest that activity in RPE-related regions, including the VS and SN/VTA, represents various types of RPE and that neural representation is modulated by the intensity or value (positive/negative) of RPE.

Face memories are enhanced by outcomes of face-based social rewards such as smiling and highly attractive faces (for review, see Dolcos et al., 2017; Tsukiura, 2012), and the memory enhancement is involved in the interaction between the orbitofrontal cortex (OFC), related to the processing of face-based social rewards (for review, see Padoa-Schioppa and Cai, 2011), and the hippocampus (HC), related to memory (Tsukiura and Cabeza, 2008, 2011a). Another fMRI study demonstrated that decreasing signals of monetary RPE in the VS was associated with enhanced functional connectivity between the RPE-related VS and the memory-related HC (Wimmer et al., 2014). Thus, functional networks between RPE-related regions such as the VS or SN/VTA and memory-related regions such as the HC could contribute to the enhancement of face memories due to RPE in facial attractiveness.

In the present fMRI study, we scanned healthy young adult males to investigate the neural mechanism underlying RPE-induced improvement in face memories in social rewards derived from facial attractiveness. Based on previous studies, we made two predictions. First, univariate activity in RPE-related regions, including the VS and SN/VTA, would exhibit linear increases as a linearly increasing function from negative RPE to non-RPE to positive RPE in facial attractiveness. In addition, given that the VS activity reflects the increasing function from negative RPE to positive RPE but not the decreasing function (Pine et al., 2018), multivariate activity patterns in these regions would discriminate between positive and negative RPE in facial attractiveness. Second, functional connectivity patterns between RPE-related regions and the memory-related HC during the successful encoding of face memories would be different between positive and negative RPE in facial attractiveness.

2. Materials and methods

2.1. Participants

We scanned 45 male undergraduate and graduate students (mean age = 21.04 years, SD = 1.59) from the Kyoto University community and paid them for their participation in the fMRI experiment. All participants were healthy, right-handed, native Japanese speakers with no history of neurological or psychiatric diseases. Their handedness was confirmed by the Japanese version of the FLANDERS handedness questionnaire (Nicholls et al., 2013; Okubo et al., 2014). Participants had normal vision or vision corrected to normal with MRI-compatible glasses. The sample size was computed with an a priori power analysis in G*Power version 3.1 (Faul et al., 2007); this estimated a total sample size of 36 with the following parameters: medium effect size ($f = 0.25$), error probability of $\alpha = .05$, and power of 0.90. To retain enough statistical power after excluding data due to poor performance, excessive head motion, and so on, we recruited 45 young adult males for the present study. All participants provided informed consent to participate, and the protocol was approved by the Institutional Review Board (IRB) of Graduate School of Human and Environmental Studies, Kyoto University (20-H-37).

To assess individual psychological and neuropsychological characteristics, we administered several psychological and neuropsychological tests, including the Autism-Spectrum Quotient (AQ; Baron-Cohen et al., 2001; Wakabayashi et al., 2004), the Center for Epidemiologic Studies Depression scale (CES-D; Radloff, 1977; Shima et al., 1985), and the Japanese version of the 20-item Prosopagnosia Index (PI20-J; Nakashima et al., 2020; Shah et al., 2015). The CES-D and AQ data were not included in the analyses. One participant was classified as exhibiting moderate developmental prosopagnosia on the PI20-J (n = 1). Six participants data met the fMRI exclusion criteria: large head motion (n = 2), possible pathological structural changes (n = 3: two probable arachnoid cysts and one abnormally large ventricle), and electrical artifacts (n = 1). Three participants met the behavioral performance criteria: no response trials more than 2 SD of the mean in all participants (n = 2) and fewer trials than one hit trial in any experimental condition (n = 1). In addition, one participant data was excluded due to PC malfunction (n = 1). After applying the exclusion criteria, data from 10 participants were excluded from all behavioral and fMRI analyses (two exclusion criteria were applied to one participant). Finally, data from 35 participants (mean age = 21.14 years, SD = 1.54) were analyzed in the present study.

2.2. Stimuli

A total of 227 unfamiliar female faces with neutral expressions were selected from previous studies with permission from the corresponding authors (Oikawa et al., 2012; Ueda et al., 2018). The rationale for using male participants only was that the potential effect of RPE in facial attractiveness on memory for faces was larger for male participants than for female participants in the pilot studies for female stimuli. All stimuli were retouched in Adobe Photoshop CS 5 (www.adobe.com). After the image quality was adjusted, all stimuli were rotated to level the eye tilt, and then the facial contours were corrected. Colored facial images were converted into grayscale images with dimensions of 256 × 256 pixels on a white background. Easily identifiable visual features, including distinctive clothes, body parts shown below the shoulders, blemishes, freckles, moles and accessories, were removed. The eyes and their periphery in each facial image were digitally applied cosmetics with SNOW (www.snowcorp.com).

To choose stimuli for use in the present study, each face was rated on perceived facial attractiveness, valence (of facial expression) and arousal (of facial expression) by 20 healthy male undergraduate and graduate students (mean age = 21.90 years, SD = 1.80) recruited from the Kyoto University community; these students did not participate in the fMRI experiment. For the subjective ratings, 8-point rating scales were employed (facial attractiveness: from 1 = very unattractive to 8 = very attractive; valence: from 1 = very negative to 8 = very positive; and arousal: from 1 = very weak to 8 = very strong). Facial stimuli were presented individually at random; stimulus was presented for 2.0 s with a 0.5 s interstimulus interval (ISI). Each rating was performed in separate runs, and the order of each run was counterbalanced across participants.

According to these rating scores, we selected 168 facial stimuli for the fMRI experiment. The mean and SD of rating scores for each face were computed in each rating category. First, facial stimuli with SD above +2 SD from the mean SD of all stimuli in facial attractiveness, scores higher than 5 in arousal, or scores above ±2 SD from the mean scores of all stimuli in valence were excluded. Second, the candidate stimuli were divided into three lists: high-, moderate-, and low-attractiveness faces. Each list included 42 target faces and 14 distracter faces, which were presented only during the retrieval task. The facial attractiveness ratings were compared among the lists with a one-way analysis of variance (ANOVA). The ANOVA showed a significant

effect of list [$F(2,165) = 593.67$, $p < .001$, $\eta^2 = .88$], and post hoc tests by the Bonferroni method demonstrated that facial attractiveness significantly increased from the low-attractiveness faces to moderate-attractiveness faces to high-attractiveness faces ($p < .001$ in all contrasts). In addition, using two-tailed two-sample *t*-tests, no significant differences between target and distracter faces were found in any list [high-attractiveness faces: $t(54) = 0.56$, $p = .58$, $d = 0.17$; moderate-attractiveness faces: $t(54) = 0.43$, $p = .67$, $d = 0.13$; low-attractiveness faces: $t(54) = 0.40$, $p = .69$, $d = 0.12$]. Images of target faces covered by a white shield except for around the eyes were generated with Adobe Photoshop CS 5; an area of 110 × 30 pixels around their eyes was shown. This manipulation of facial stimuli helped participants to induce substantial errors in predicting facial attractiveness for partially covered faces.

2.3. Experimental procedures

All participants performed the encoding, retrieval and evaluation tasks. Neural activity was measured only in the encoding task, and behavioral data were collected on a Windows PC in all tasks. The fMRI scan during encoding trials followed an event-related method. Stimulus presentation and recording of behavioral responses in all tasks were controlled by MATLAB (www.mathworks.com). Button responses were collected by MRI-compatible buttons in the encoding task during fMRI scans and by a keyboard on Windows PC in the retrieval and evaluation tasks (not during fMRI scans). All participants were fully trained on experimental procedures in all tasks.

2.3.1. Encoding task

An example of encoding trials is shown in Fig. 1. Each trial included two phases, prediction and outcome. In the prediction phase, participants were presented with a target face, which was covered by a white shield except for around the eyes, and were required to predict the attractiveness of the face after the white shield was removed. The predicted facial attractiveness was indicated on an 8-point rating scale (from 1 = very unattractive to 8 = very attractive). In the outcome phase, participants were presented with the same face after the white shield was removed and required to rate observed facial attractiveness on the same 8-point scale. Each face was presented for 2.5 s in the prediction phase and for 3.5 s in the outcome phase. A visual fixation was presented as ISI or intertrial interval (ITI), jittered with variable duration (2.5 s – 5.5 s). Each response (subjective rating of facial attractiveness) was recorded by pressing one of eight buttons as soon as possible. The assigned buttons for the attractiveness ratings were ascending for half of the participants and descending for the other half. This manipulation was used to cancel out the effect of motor-related activation related to button pressing. Each run of the encoding task included 42 trials, and three runs were prepared to encode all target faces on the three lists. Thus, 126 faces were viewed through three runs in the encoding task, in which facial attractiveness was rated in both prediction and outcome phases. No instruction that memory for faces was tested in the later retrieval task was provided to participants.

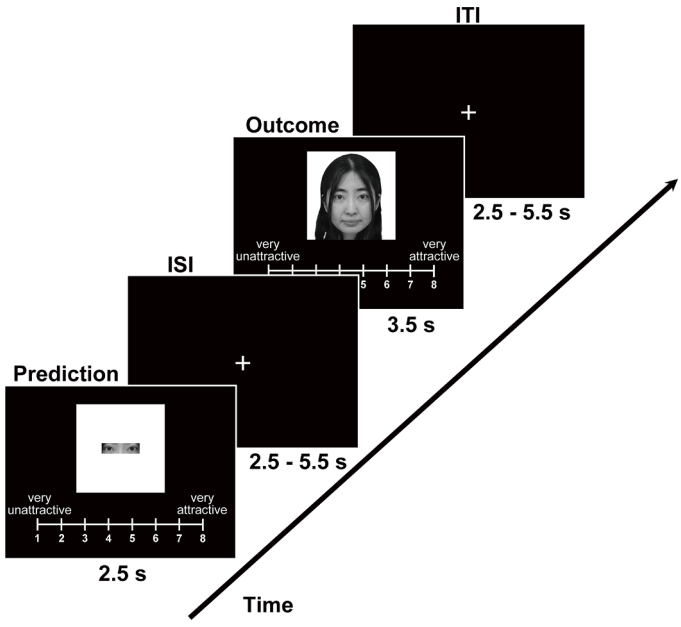

Fig. 1. An example of the encoding trial. In the prediction phase, participants were presented with a face covered by a white shield except for around the eyes and were required to predict the facial attractiveness of that face after the white shield was removed. In the outcome phase, participants were presented with the same face after the white shield was removed, and required to rate the facial attractiveness. In both phases, participants were instructed to rate the facial attractiveness on an 8-point scale (from 1 = very unattractive to 8 = very attractive). The face picture in this figure is for illustration purposes only. All labels were presented in Japanese. English is used here for illustration purposes only.

RPE on each trial was defined as the difference in the facial attractiveness ratings between the prediction and outcome phases. Based on this definition, we generated three RPE conditions. Trials in which the rating scores of facial attractiveness were higher in the prediction phase than in the outcome phase (i.e., predicted facial attractiveness > observed facial attractiveness) were categorized as negative RPE (RPE−). In contrast, trials with lower scores of facial attractiveness in the prediction phase than in the outcome phase (i.e., predicted facial attractiveness < observed facial attractiveness) were categorized as positive RPE (RPE+). Trials in which there was no difference in the ratings of facial attractiveness between the prediction and outcome phases (i.e., predicted facial attractiveness = observed facial attractiveness) were labeled as non-RPE (RPE±).

2.3.2. Retrieval task

Approximately twenty minutes after the encoding task, participants performed the retrieval task on a Windows PC outside the MRI scanner. During the retrieval task, participants were randomly presented with 126 target and 42 distracter faces one by one and were required to judge whether or not the faces were presented in the encoding task. The recognition judgment was accompanied by four response options with two levels of confidence: definitely old, probably old, probably new, definitely new. These responses were recorded by pressing one of four keys as soon as possible. Each face was presented for 2.5 s and was followed by a visual fixation as jittered ISI (0.5 s – 3.5 s). The retrieval task included 168 trials, which were performed in one run. Trials in which participants did not respond in the prediction phase and/or in the outcome phase during encoding and trials with no response during retrieval were excluded from all analyses. The retrieval trials in which "definitely old" or "probably old" were provided for target faces were defined as Hit; conversely, the retrieval trials in which "probably new" or "definitely new" were provided for target faces were defined as Miss. Thus, using this categorization in the retrieval trials, the encoding trials were classified into subsequently remembered (Subsequent hit) and subsequently forgotten (Subsequent miss) (Paller and Wagner, 2002). The Subsequent hit and Subsequent miss trials were further divided into three conditions categorized by RPE (RPE−, RPE±, and RPE+ in each of Subsequent hit and Subsequent miss).

2.3.3. Evaluation task

Immediately after the retrieval task, participants were required to rate the perceived facial attractiveness, trustworthiness, valence, and arousal of faces presented in the encoding and retrieval tasks. These ratings were performed in separate runs for each category. To rate facial attractiveness, participants were randomly presented with the 42 distracter faces one by one, and were required to rate how attractive each

face was on an 8-point scale (from 1 = very unattractive to 8 = very attractive). To rate other variables, participants were randomly presented with 126 target and 42 distracter faces one by one, and rated each face on an 8-point scale (trustworthiness: from 1= very untrustworthy to 8 = very trustworthy; valence: from 1 = very negative to 8 = very positive; and arousal: from 1 = very weak to 8 = very strong). These responses were recorded by pressing one of eight keys as soon as possible. Each face was presented for 2.0 s and was followed by a visual fixation presented for a fixed ISI of 0.5 s. The order of these rating runs was counterbalanced across participants.

2.4. MRI data acquisition

Structural and functional MRIs were acquired by a MAGNETOM Verio 3T MRI scanner with a 32-channel head coil (Siemens, Erlangen, Germany) at Institute for the Future of Human Society, Kyoto University. Stimuli were visually presented on an MRI-compatible display (BOLD screen 32 LCD, Cambridge Research Systems, Rochester, UK) and were viewed through a mirror attached to the head coil of the MRI scanner. Scanner noise was diminished by ear plugs, and head motion during scanning was minimized by a neck supporter and foam pads. An 8-button fiber-optic response device (8-button Bimanual Curved Lines, Current Designs, Philadelphia, USA), which consisted of two response boxes with four buttons each, was used to record behavioral responses in the encoding task with fMRI scanning.

During MRI scanning, first, three directional T1-weighted structural images were collected to localize functional and high-resolution anatomical images. Second, gradient-echo echo-planar images (EPI), which are sensitive to blood oxygenation level-dependent (BOLD) contrast, were acquired for functional images [repetition time (TR) = 1000 ms, flip angle (FA) = 60°, echo time (TE) = 30.6 ms, field of view (FOV) = 22.8 cm × 22.8 cm, matrix size = 76 × 76, slice thickness/gap = 3.0/0 mm, 56 horizontal slices, multiband factor = 4]. Finally, high-resolution T1-weighted structural images were obtained by MPRAGE (TR = 2250 ms, TE = 3.51 ms, FOV = 25.6 cm × 25.6 cm, matrix size = 256 × 256, slice thickness/gap = 1.0/0 mm, 208 horizontal slices).

2.5. fMRI data analysis

2.5.1. Preprocessing

The preprocessing of fMRI data was performed with Statistical Parametric Mapping 12 (SPM12) implemented in MATLAB (www.mathworks.com). For preprocessing, first, the initial eight volumes in each run were discarded to prevent an initial dip, and then six parameters reflecting head motion were extracted from a series of the remaining functional images (realignment). Second, a volume of high-resolution structural images was coregistered to the first volume of functional images (coregistration). Third, parameters to fit the coregistered structural images to the tissue probability map (TPM) in the Montreal Neurological Institute (MNI) template were estimated, and the parameters were applied to all functional images (resampled resolution = 3.0 mm × 3.0 mm × 3.0 mm) (spatial normalization). Finally, these normalized functional images were spatially smoothed using a 7.0 mm FWHM Gaussian kernel (spatial smoothing). These functional images were used in univariate and functional connectivity analyses, and those without spatial smoothing were used for multivariate pattern analysis (MVPA).

2.5.2. ROI definition

In the present study, we focused on activity in two regions of interest (ROIs): the extended VS and the HC. The extended VS ROI was defined as a region shared between an anatomical mask image of the bilateral striatum (Tziortzi et al., 2011), SN and VTA (Murty et al., 2014) and a functional image extracted from the term-based meta-analysis of Neurosynth (Yarkoni et al., 2011), in which a functional map was generated by the terms "reward", "rewards", and "rewarding" used in previous functional neuroimaging studies. The HC ROI related to successful encoding was anatomically defined as a region including the bilateral HC (for review, see Henson, 2005; Paller and Wagner, 2002; Spaniol et al., 2009; Sugar and Moser, 2019), which was extracted from the Harvard-Oxford subcortical structural atlas (Desikan et al., 2006; Frazier et al., 2005; Goldstein et al., 2007; Makris et al., 2006).

2.5.3. Univariate analysis

In the univariate analysis, we employed SPM12 to analyze functional images at the individual level and at the group level. In the individual-level (fixed-effect) analysis, trial-related activity in each of the prediction and outcome phases was modeled by convolving an onset vector with a canonical hemodynamic response function (HRF) with the general linear model (GLM). In this model, the time that each face was presented in both prediction and outcome phases was defined as the individual onset, and the event duration was set to 0 s. Six parameters reflecting head motion and magnetic field drift were included in this model as confounding factors.

Two models were analyzed in the univariate analysis. First, activation that increased in linear manner with increased RPE and activation that increased with both positive and negative RPE were estimated by parametric modulation analysis, which enabled us to identify activation reflecting functions estimated from regressors related to experimental parameters (Büchel et al., 1998). In this analysis, trial-by-trial regressors of linear (RPE−: 1, RPE±: 2, RPE+: 3) and V-shaped (RPE−: 2, RPE±: 1, RPE+: 2) functions were applied to individual trials in the outcome phase during encoding, and beta estimates reflecting these functions were deconvolved from all voxels in the whole brain. The model yielded *t*-contrasts reflecting the value and intensity of RPE in each participant. Second, successful encoding activation was modeled in the outcome phase of each encoding trial. All encoding trials were divided into the Subsequent hit and Subsequent miss trials. Significant activation reflecting successful encoding was defined as a *t*-contrast of the Subsequent hit vs. Subsequent miss trials, and the contrast image was created for each participant.

In the group-level (random-effect) analysis, contrast images estimated with the individual-level analysis were statistically tested with one-sample *t*-tests. First, significant activation reflecting linear increases or decreases with increased RPE was identified by applying positive and negative values to *t*-contrasts related to the RPE-related increasing function (RPE−: 1, RPE±: 2, RPE+: 3). In addition, significant activation reflecting the intensity of RPE was found by applying a positive value to *t*-contrasts related to the RPE-related V-shaped function (RPE−: 2, RPE ±: 1, RPE+: 2). Second, successful encoding activation was identified by a one-sample *t*-test for contrast images of Subsequent hit vs. Subsequent miss. The height threshold at the voxel level ($p < .001$) was corrected for multiple comparisons with a minimum cluster size of two contiguous voxels in the predefined ROIs (FWE, $p < .05$), which included the bilateral extended VS ROI when analyzing regions related to the value and intensity of RPE and the bilateral HC ROI when analyzing regions related to successful encoding.

2.5.4. MVPA

In MVPA, using Pattern Recognition of Neuroimaging Toolbox (PRoNTo) version 2.1 (Schrouff et al., 2013) implemented in MATLAB, we investigated how multivariate activity patterns in the bilateral extended VS ROI represent information of RPE in facial attractiveness.

Before MVPA, using SPM12, trial-by-trial activity in both prediction and outcome phases was estimated for individual participants by new GLMs in each run (Mumford et al., 2014; Mumford et al., 2012; Rissman et al., 2004). The models were estimated by convolving an onset vector with a canonical HRF, in which the trial onset with an event duration of 0 s was set as the time at which each face was presented in both prediction and outcome phases. The GLM included a regressor for a specific single trial in each of the prediction and outcome phases and regressors for all the other trials in both phases, and the model was estimated for all

individual trials in each run. In addition, six parameters reflecting head motion and magnetic field drift were included in the models of individual trials as confounding factors. For each participant, these models generated a new map of beta estimates for the whole brain in individual trials, and the trial-by-trial beta images were applied to MVPA by PRoNTo. In this analysis, functional images from two participants were excluded from data sets to be analyzed, because in any one of the RPE conditions, they showed fewer trials than two trials in one run. Thus, functional images from 33 participants were applied to MVPA.

In the MVPA classification analysis, first, for each participant, we created a whole-brain mask in which voxels without beta values were excluded and performed pattern classification analyses by PRoNTO in this whole-brain mask. The features were extracted from all voxels in the extended VS ROI and were centered according to the mean of the training data for each voxel (mean centering). Three patterns of binary classification (RPE+ vs. RPE±, RPE− vs. RPE±, and RPE+ vs. RPE−) were computed by support vector machine (SVM) with a linear kernel in all voxels of the extended VS ROI. Training and testing followed a leave-one-run-out cross-validation procedure, in which data from two runs were applied for training and data from the one remaining run were applied for testing. Mean classification accuracy defined by balanced accuracy (BA) was analyzed for the ROI in each participant, and the mean BA values were analyzed by one-tailed one-sample *t*-tests, which tested whether multivariate activity patterns in the ROI significantly discriminated between the two RPE conditions at above the chance level (50 %). Significant results in one-sample *t*-tests were verified by 1000 times permutation tests. In the permutation tests, pattern classification analyses were repeated 1000 times on data, in which labels of two classes to be classified were randomly swapped. This manipulation yielded a null distribution, in which the two RPE conditions were not represented by multivariate activity patterns in the extended VS ROI.

2.5.5. Functional connectivity analysis

To examine how functional connectivity during successful encoding was modulated by differences in RPE, functional connectivity between regions related to RPE and successful encoding was investigated in each RPE condition. Functional connectivity was analyzed by a generalized form of context-dependent psychophysiological interactions (gPPI; McLaren et al., 2012). In the preprocessing before the gPPI analysis, three encoding runs were collapsed into one run, and trial-related regressors in both prediction and outcome phases of six conditions, which were created by the combination of the RPE condition (RPE−, RPE±, and RPE+) and subsequent memory (Subsequent hit and Subsequent miss), were remodeled by convolving onset vectors with a canonical HRF in the context of GLM, in which trial onsets with an event duration of 0 s were set as the time at which each face was presented in both prediction and outcome phase. This model also included no-response trials as a condition and six parameters related to head motion and magnetic field drift as confounding factors. Seed regions for the functional connectivity analysis were determined from regions in the bilateral VS that showed significant activation as a linear function of increases in RPE and those in the bilateral HC that reflected successful encoding activation in univariate analysis. These seeds were defined as volumes of interest (VOIs) with a sphere of 6 mm radius at the center of the peak voxel identified in the univariate analysis. The seed VOIs in the left HC (x = -18, y = -7, z = -19) and right HC (x = 18, y = -7, z = -19) were not identified from the data of two participants. In addition, seed VOIs in the left VS (x = -15, y = 8, z = -7) were not identified in four participants, seed VOIs in the left VS (x = -9, y = 8, z = -4) were not identified in three participants, and seed VOIs in the right VS (x = 15, y = 11, z = -4) were not identified in three participants. Thus, functional connectivity with the left HC (x = -18, y = -7, z = -19) and right HC (x = 18, y = -7, z = -19) was analyzed in 33 participants, functional connectivity with the left VS (x = -9, y = 8, z = -4) and right VS (x = 15, y = 11, z = -4) was analyzed in 32 participants, and functional connectivity with the left VS (x = -15, y = 8, z = -7) was analyzed in 31 participants.

Region-to-region functional connectivity was analyzed by the gPPI toolbox (www.nitrc.org/projects/gppi), which creates models at the individual-level. In the individual-level (fixed-effect) analysis, the models were estimated with a design matrix including (1) six condition regressors (RPE−/Subsequent hit, RPE−/Subsequent miss, RPE±/Subsequent hit, RPE±/Subsequent miss, RPE+/Subsequent hit and RPE+/Subsequent miss) formed by convolving vectors of condition-related onsets with a canonical HRF, (2) time-series BOLD signals extracted from the seed VOI, and (3) PPI regressors as the interaction between (1) and (2). In addition, six parameters related to head motion and magnetic field drift were also included in the models as confounding factors. Linear contrasts were computed in the models for each seed region, and regions showing a significant effect in *t*-contrasts of the PPI regressors were considered functionally connected with each seed region. Six contrast images related to the PPI regressors were obtained for each participant (RPE−/Subsequent hit, RPE−/Subsequent miss, RPE ±/Subsequent hit, RPE±/Subsequent miss, RPE+/Subsequent hit and RPE+/Subsequent miss), and these contrast images were applied in the group-level analysis.

In the group-level (random-effect) analysis, regions showing significant functional connectivity with seed regions were explored during successful encoding of faces in each RPE condition. One-sample *t*-tests of each RPE condition were performed in the PPI regressor contrasts of Subsequent hit masked exclusively by those of Subsequent miss. In these analyses, the height threshold at the voxel level ($p < .001$) was corrected for multiple comparisons in the bilateral extended VS ROI for the HC seeds and the bilateral HC ROI for the VS seeds (FWE, $p < .05$) with a minimum cluster size of two contiguous voxels.

2.6. Data/code availability statement

Behavioral data, ROI images, BA values in MVPA and statistical maps in the univariate and functional connectivity analyses are available through the Open Science Framework (https://osf.io/5esnj). Due to the lack of participant consent, raw structural and functional MRI data cannot be shared publicly. Sharing of these data may be considered upon a data use agreement (DUA) that is required under circumstances where data privacy can be assured.

3. Results

3.1. Behavioral results

Table 1 summarizes the behavioral data. First, mean hit rates were calculated as proportions of the Hit trials out of the Hit and Miss trials. A one-way repeated-measures ANOVA for hit rates was analyzed with a factor of RPE condition (RPE−, RPE±, and RPE+). There was a significant effect of RPE condition [$F(2,68) = 6.67$, $p = .002$, $\eta^2 = .16$]. In post hoc tests by the Bonferroni's methods, we found significantly higher hit rates in RPE+ than in RPE± ($p = .002$, $d = 0.64$). However, there was no significant difference between RPE− and RPE± ($p = .084$, $d = 0.40$), and

Table 1
Behavioral results.

	RPE− (SD)	RPE± (SD)	RPE+ (SD)
Proportion of retrieval accuracy			
Hit rate	0.53 (0.13)	0.48 (0.12)	0.56 (0.13)
FA rate		0.19 (0.10)	
Number of trials during encoding (Outcome phase)			
Subsequent hit	22.97 (11.46)	16.57 (6.28)	26.66 (12.12)
Subsequent miss	20.49 (10.75)	17.77 (7.01)	20.71 (9.98)
Rating score			
Trustworthiness	4.13 (0.55)	4.43 (0.63)	4.86 (0.60)
Valence	4.59 (0.47)	4.92 (0.57)	5.37 (0.48)
Arousal	3.47 (0.72)	3.79 (0.78)	4.22 (0.86)

RPE = reward prediction error; SD = standard deviation; FA = false alarm.

between RPE+ and RPE− ($p = .52$, $d = 0.24$). The results of hit rates in each RPE condition are illustrated in Fig. 2.

To investigate whether face-based social signals other than facial attractiveness were different among the RPE conditions, perceived facial trustworthiness, valence and arousal for target faces were analyzed by one-way repeated-measures ANOVAs with a factor of RPE condition (RPE−, RPE±, and RPE+). Regarding perceived facial trustworthiness, a significant effect of RPE condition was identified [$F(2,68) = 34.65$, $p < .001$, $\eta^2 = .50$], and post-hoc tests showed significantly higher facial trustworthiness in RPE+ than in RPE± ($p < .001$, $d = 0.72$) and RPE− ($p < .001$, $d = 1.23$) and significantly higher facial trustworthiness in RPE± than in RPE− ($p = .003$, $d = 0.52$). Regarding valence and arousal in facial expression, we found significant effects of RPE condition [valence: $F(2,68) = 51.91$, $p < .001$, $\eta^2 = .60$; arousal: $F(2,68) = 47.13$, $p < .001$, $\eta^2 = .58$]. Post-hoc tests in both valence and arousal demonstrated that facial expression in RPE− was the most negative in valence (RPE± vs. RPE−: $p < .001$, $d = 0.65$; RPE+ vs. RPE−: $p < .001$, $d = 1.55$) and lowest in arousal (RPE± vs. RPE−: $p < .001$, $d = 0.41$; RPE+ vs. RPE−: $p < .001$, $d = 0.96$) and that facial expression in RPE± was the second most negative in valence (RPE+ vs. RPE±: $p < .001$, $d = 0.89$) and second lowest in arousal (RPE+ vs. RPE±: $p < .001$, $d = 0.55$). In addition, ratings of perceived facial attractiveness were compared between target and distracter faces with a two-tailed paired t-test. In this test, there was no significant difference between these face categories [$t(34) = 1.09$, $p = .28$, $d = 0.18$].

3.2. fMRI results

3.2.1. Univariate analysis

Univariate activation in the fMRI data was investigated by parametric modulation analysis, in which activation reflecting a linear increase or decrease with increased RPE and activation reflecting increases for both positive and negative RPE was analyzed in the bilateral extended VS ROI. The VS exhibited significant linear increases in activation with increased RPE in facial attractiveness (Fig. 3). However, the bilateral extended VS ROI did not exhibit significant activation reflecting linear decreases with increased RPE or increases with both positive and negative RPE.

Successful encoding activation, which was defined by a contrast of Subsequent hit vs. Subsequent miss in the outcome phase, was analyzed by a one-sample t-test in the HC ROI. This analysis showed significant activation for successful encoding of face memories in the bilateral HC. Details of these univariate findings are summarized in Table 2.

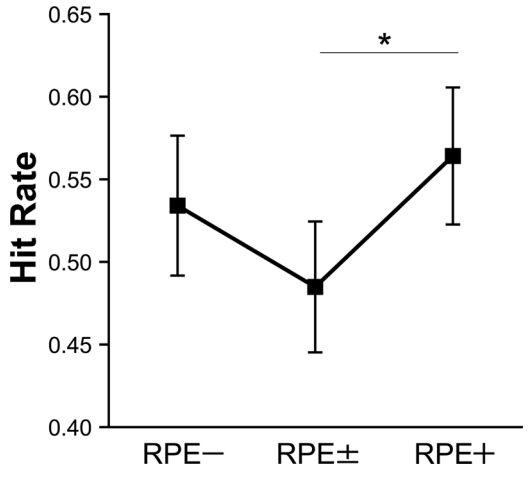

Fig. 2. Hit rates in the retrieval task. Error bars represent 95 % confidence intervals. *: $p < .01$.

3.2.2. MVPA

MVPA was used to test whether multivariate activity patterns in the bilateral extended VS ROI accurately discriminated between the RPE conditions above the chance level (50 %). As illustrated in Fig. 4, one-tailed one-sample t-tests for the BA values from individual participants demonstrated that differences between RPE− and RPE± [$t(32) = 2.17$, $p = .02$, $d = 0.38$] and between RPE+ and RPE± [$t(32) = 2.17$, $p = .02$, $d = 0.38$] were successfully classified by multivariate activity patterns in this ROI. However, a one-tailed one-sample t-test of whether multivariate activity patterns in this ROI discriminated between RPE+ and RPE− was not significant [$t(32) = 0.58$, $p = .28$, $d = 0.10$]. Significant results of the BA values in one-sample t-tests were verified by 1000 times permutation tests (RPE+ vs. RPE±: $p = .001$; RPE− vs. RPE±: $p = .002$).

3.2.3. Functional connectivity analysis

Region-to-region functional connectivity during successful encoding in each RPE condition was analyzed in seed regions of the bilateral VS and bilateral HC. Seed regions in the bilateral VS showed significant functional connectivity with regions in the bilateral HC ROI in both RPE+ and RPE−. In addition, trial-by-trial activity in the bilateral HC was functionally correlated with that in the bilateral extended VS ROI only in RPE+. These patterns of functional connectivity are shown in Fig. 5, and detailed findings are summarized in Table 3.

4. Discussion

Two main findings emerged from the present study. First, univariate activity in the VS exhibited linear increases with increasing RPE in facial attractiveness as a social reward, and multivariate activity patterns in the extended VS ROI significantly discriminated between RPE+/RPE− and RPE± during the processing of facial attractiveness as a social reward. Second, significant functional connectivity during successful encoding of faces was identified between the RPE-related VS and the memory-related HC ROI in RPE+ and RPE− and between the HC and the RPE-related extended VS ROI only in RPE+. These findings suggest that the enhancement of face memory induced by face-based social RPE is due to the interaction of the VS and SN/VTA, which represent RPE information, with the HC, which is related to successful encoding. In addition, this interaction could be modulated by positive and negative RPE in facial attractiveness as a social reward. These findings are discussed in separate sections below.

4.1. Neural representation related to the processing of RPE in facial attractiveness as a social reward

The first main finding of the present study was that univariate activity in the VS exhibited a significant linear increase with increasing RPE in facial attractiveness as a social reward, and multivariate activity patterns in the extended VS ROI, including the VS and SN/VTA, significantly discriminated between RPE+/RPE− and RPE±. These findings suggest that the intensity of activation in the VS is modulated by increases in face-based social RPE and that RPE in facial attractiveness as a social reward is represented by multivariate activity patterns in RPE-related regions such as the VS.

The present finding that univariate activation in the VS exhibited a linear increase with increasing face-based social RPE is consistent with previous functional neuroimaging studies. For example, significant activation in the VS has been observed in both social and monetary RPE (Häusler et al., 2015; Lin et al., 2012). Other studies investigating RPE in monetary rewards have demonstrated that VS activation reflects a linear increase in RPE (Abler et al., 2006; Cao et al., 2019) and the intensity and value (positive/negative) of RPE (Fouragnan et al., 2018; Pine et al., 2018). In addition, neurophysiological studies have reported that the excitability of dopaminergic neurons in reward-related regions is modulated by positive and negative RPE (Schultz et al., 1997; Zaghloul et al., 2009). For example, in macaques, firing rates of dopaminergic

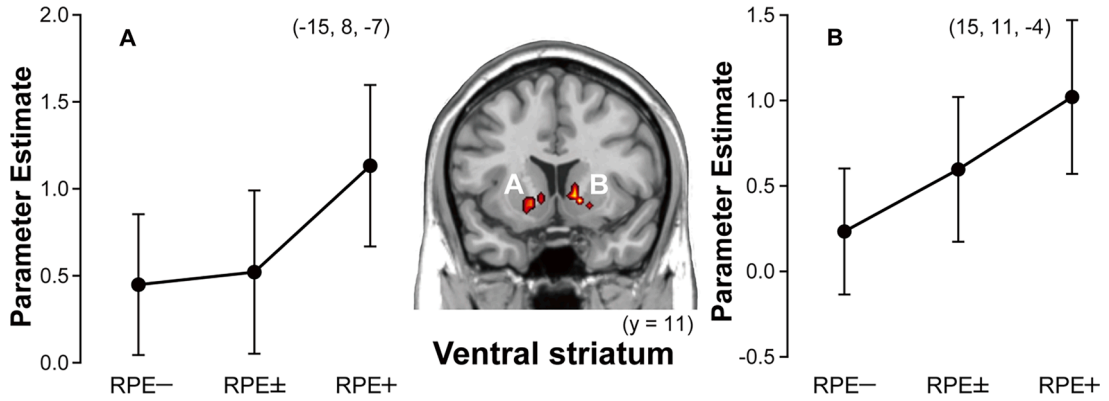

Fig. 3. Results of univariate analysis. Regions showing significant activation reflecting linear increases with increased RPE in the extended VS region of interest (ROI). Beta values of parameter estimates in graphs were extracted from the peak voxel of activation clusters. (A) Univariate activation in the left VS. (B) Univariate activation in the right VS. Error bars represent 95 % confidence intervals.

Table 2
Regions showing significant activation in univariate analysis.

		MNI coordinates				
Region	L/R	x	y	z	Z value	*k*
Linear increase with increased RPE in the extended VS ROI						
Caudate nucleus/Putamen	R	15	11	-4	5.83	19
Putamen	L	-15	8	-7	4.80	12
Caudate nucleus	L	-9	8	-4	4.18	6
Linear decrease with increased RPE in the extended VS ROI						
No significant activation was identified.						
V-shaped increase with positive and negative RPE in the extended VS ROI						
No significant activation was identified.						
Subsequent hit vs. Subsequent miss in the hippocampal ROI						
Hippocampus	L	-18	-7	-19	4.49	5
Hippocampus	R	18	-7	-19	4.16	5

RPE = reward prediction error; L = left; R = right; k = cluster size; ROI = region of interest; VS = ventral striatum; MNI = Montreal Neurological Institute.

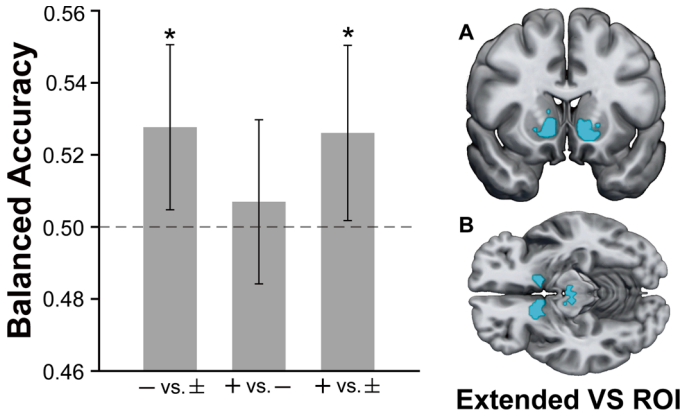

Fig. 4. Results of multivariate pattern analysis (MVPA). (A) Coronal image of the extended VS region of interest (ROI). (B) Horizontal image of the extended VS ROI. The graph shows the mean classification accuracies (balanced accuracies) from the classification analyses between the RPE conditions. Error bars represent 95 % confidence intervals, and the dotted line corresponds to the chance level (50 %). VS = ventral striatum, − = RPE−, ± = RPE±, + = RPE+. *: $p < .05$.

neurons in the VTA increased for positive RPE and decreased for negative RPE; such responses were not observed when no RPE occurred (Schultz et al., 1997). A similar finding was reported in an fMRI study of human participants: VS activity was enhanced when RPE in facial attractiveness as a social reward was positive, whereas VS activity was inhibited when the face-based social RPE was negative (Bray and O'Doherty, 2007). Thus, the present univariate findings suggest that VS activation reflects changes in the excitability of dopaminergic neurons in the VS, which is modulated by positive or negative RPE.

In MVPA, we found that multivariate activity patterns in the RPE-related regions, including the VS and SN/VTA, successfully discriminated between the presence and absence of RPE in facial attractiveness as a social reward. This finding is consistent with a meta-analysis that demonstrated significant activation in VS clusters for both positive and negative RPE (Garrison et al., 2013). In addition, fMRI studies using MVPA have reported that information on monetary and social rewards was represented by multivariate activity patterns in the VS (Wake and Izuma, 2017), and activity patterns in this region significantly distinguished between monetary rewards and social rewards (Clithero et al., 2011). Thus, activity patterns in RPE-related regions, including the VS and SN/VTA, could represent information about the generation of face-based social RPE during the processing of faces.

4.2. Neural mechanisms underlying RPE modulation of face memories in facial attractiveness as a social reward

The second main finding of the present study was that region-to-region functional connectivity between the RPE-related regions, including the VS and SN/VTA, and the memory-related HC was the highest when faces were successfully encoded with positive RPE in facial attractiveness. This finding suggests that the memory enhancement by face-based social RPE is involved in the interaction between RPE-related regions and the HC, and that this interaction is strengthened by positive RPE in facial attractiveness as a social reward.

Functional connectivity patterns in the present study are consistent with the results of a previous fMRI study that employed a paradigm of RPE-dependent reinforcement learning and episodic memory using monetary rewards; increasing functional connectivity was observed between the VS related to the reward-dependent learning and the HC related to the episodic memory formation during the successful encoding of object images (Wimmer et al., 2014). The reward-related enhancement of episodic memories in both monetary and social contexts has been observed in both outcome and anticipation phases of rewards, and the importance of interactions between the HC and reward-related regions, including the OFC, VS, and SN/VTA, in the memory enhancement has been consistently identified in functional neuroimaging studies (Adcock et al., 2006; Frank et al., 2019; Schott et al., 2004; Shigemune et al., 2014; Shigemune et al., 2017; Sugimoto et al., 2021; Tsukiura and Cabeza, 2008, 2011a; Wittmann et al., 2005). The reward-related memory enhancement has been explained by potential mechanisms that dopaminergic inputs to the HC promote protein synthesis associated with synaptic plasticity (Smith et al., 2005) and

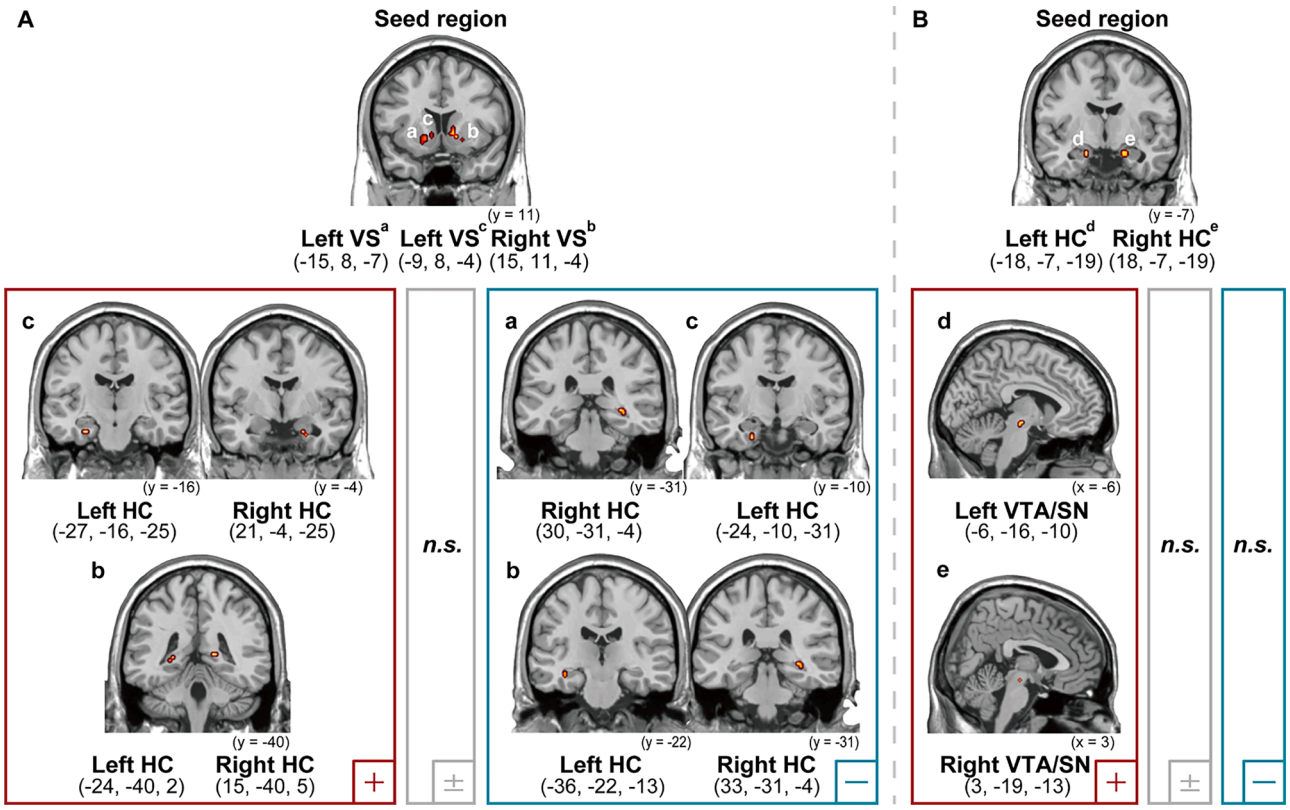

Fig. 5. Results of functional connectivity analysis. (A) Functional connectivity between the VS seeds and the HC region of interest (ROI) in each RPE condition. (B) Functional connectivity between the HC seeds and the extended VS ROI in each RPE condition. VS = ventral striatum, HC = hippocampus, VTA = ventral tegmental area, SN = substantia nigra, − = RPE−, ± = RPE±, + = RPE+.

Table 3
Results of functional connectivity analysis.

Region	Condition	MNI coordinates x	y	z	Z value
Left VS seed (-15, 8, -7)					
Hippocampus	RPE−	30	-31	-4	4.89
Left VS seed (-9, 8, -4)					
Hippocampus	RPE+	21	-4	-25	4.24
Hippocampus	RPE+	-27	-16	-25	4.21
Hippocampus	RPE+	21	-40	5	4.13
Hippocampus	RPE−	-24	-10	-31	4.64
Right VS seed (15, 11, -4)					
Hippocampus	RPE+	15	-40	5	4.41
Hippocampus	RPE+	-24	-40	2	4.23
Hippocampus	RPE+	-33	-16	-16	4.17
Hippocampus	RPE−	33	-31	-4	4.77
Hippocampus	RPE−	-36	-22	-13	3.95
Left HC seed (-18, -7, -19)					
SN/VTA	RPE+	-6	-16	-10	4.25
Right HC seed (18, -7, -19)					
SN/VTA	RPE+	3	-19	-13	3.46

RPE = reward prediction error; HC = hippocampus; VS = ventral striatum; SN = substantia nigra; VTA = ventral tegmental area; MNI = Montreal Neurological Institute.

contribute to the induction and maintenance of late-phase long-term potentiation (LTP) (for review, see Jay, 2003; Lisman et al., 2011; Shohamy and Adcock, 2010). In addition, anatomical connectivity between the reward-related regions and the HC has been shown in experimental animals. For example, neuroanatomical studies in rats and cynomolgus monkeys have demonstrated that dopaminergic neurons in the VTA project directly to the HC (Gasbarri et al., 1994; Samson et al., 1990) and that anatomical loops including the HC, VS, and VTA are important in regulating the entry of information into long-term memory (for review, see Lisman and Grace, 2005). A diffusion tensor imaging (DTI) study in human participants showed white matter connectivity between the HC and VS (Lei et al., 2014). Thus, the present findings of functional connectivity between the RPE-related VS-SN/VTA and the memory-related HC suggest that reward-related processing in dopaminergic neurons of the VS and SN/VTA promotes memory-related LTP through interactions between the VS-SN/VTA and HC. The interaction could act as a core system for the modulation of face memories by face-based social RPE and could be differentially modulated by positive or negative RPE in facial attractiveness as a social reward.

4.3. Limitations

There was a possible limitation in the present study. As shown in behavioral results, there was significant difference in the ratings of facial trustworthiness, valence and arousal of facial expression among the RPE conditions. In the additional correlation analyses, we found that correlations between the RPE values and rating scores in the evaluation task were significant in all rating categories across individual facial stimuli (trustworthiness: $r = .61, p < .001$; emotional valence: $r = .56, p < .001$; emotional arousal: $r = .54$, $p < .001$). These findings imply that the memory enhancement in RPE+ might be affected by the possible effects of face-based socioemotional signals including the trustworthiness, emotional valence and arousal. Previous studies have reported that highly attractive faces are regarded as highly trustworthy faces (Oosterhof and Todorov, 2008), and that significant correlations with the ratings of facial attractiveness were found in the valence and arousal ratings of facial expression (Garrido and Prada, 2017). Thus, further studies would be required to cancel out the potential artifacts by face-based socioemotional signals other than RPE derived from facial attractiveness in face memories.

5. Conclusion

In the present study, using event-related fMRI, we investigated neural mechanisms underlying the modulation of face memories by RPE in facial attractiveness as a social reward. Two main findings emerged from the present study. First, univariate activity in the VS during face encoding exhibited a linear increase with increasing RPE in facial attractiveness, and multivariate activity patterns in the extended VS regions, including the VS and SN/VTA, significantly discriminated between positive/negative RPE and non-RPE regarding facial attractiveness. Second, significant functional connectivity between the RPE-related extended VS and the memory-related HC was identified most frequently when faces were successfully encoded with positive RPE in facial attractiveness. These findings suggest that the beneficial effect of face-based RPE on face memories is involved in interacting mechanisms between the extended VS regions, which represent RPE information, and the HC, which is related to successful encoding, and that the interaction is modulated by positive and negative RPE derived from face-based social rewards.

Data and code availability

Behavioral data, ROI images, BA values and statistical maps in the univariate and functional connectivity analyses are available through the Open Science Framework (https://osf.io/5esnj). Due to the lack of participant consent, raw structural and functional MRI data cannot be shared publicly. Sharing of these data may be considered upon a data use agreement (DUA) that is required under circumstances where data privacy can be assured.

CRediT authorship contribution statement

Moe Mihara: Conceptualization, Data curation, Formal analysis, Investigation, Methodology, Software, Validation, Visualization, Writing – original draft. **Reina Izumika:** Conceptualization, Formal analysis, Methodology, Software, Validation. **Takashi Tsukiura:** Conceptualization, Formal analysis, Funding acquisition, Methodology, Project administration, Software, Supervision, Validation, Visualization, Writing – review & editing.

Declaration of Competing Interest

The authors have no conflicts of interest to declare.

Data availability

Data will be made available on request.

Acknowledgments

We thank Drs. Nobuhito Abe and Ryusuke Nakai as well as Mses. Aiko Murai and Maki Terao for their technical assistance with MRI scanning, and Drs. Hiraku Oikawa and Ryuhei Ueda for permitting us to use facial stimuli. This research was supported by JSPS KAKENHI Grant No. JP19H05312, JP20H05802, and JP21K03128 and by Kyoto University Foundation (TT). The research experiments were conducted using an MRI scanner and related facilities at Institute for the Future of Human Society, Kyoto University.

References

Abler, B., Walter, H., Erk, S., Kammerer, H., Spitzer, M., 2006. Prediction error as a linear function of reward probability is coded in human nucleus accumbens. Neuroimage 31, 790–795. https://doi.org/10.1016/j.neuroimage.2006.01.001.

Adcock, R.A., Thangavel, A., Whitfield-Gabrieli, S., Knutson, B., Gabrieli, J.D.E., 2006. Reward-motivated learning: mesolimbic activation precedes memory formation. Neuron 50, 507–517. https://doi.org/10.1016/j.neuron.2006.03.036.

Büchel, C., Holmes, A.P., Rees, G., Friston, K.J., 1998. Characterizing stimulus–response functions using nonlinear regressors in parametric fMRI experiments. Neuroimage 8, 140–148. https://doi.org/10.1006/nimg.1998.0351.

Baron-Cohen, S., Wheelwright, S., Skinner, R., Martin, J., Clubley, E., 2001. The autism-spectrum quotient (AQ): evidence from asperger syndrome/high-functioning autism, malesand females, scientists and mathematicians. J. Autism Dev. Disord. 31, 5–17. https://doi.org/10.1023/A:1005653411471.

Bray, S., O'Doherty, J., 2007. Neural coding of reward-prediction error signals during classical conditioning with attractive faces. J. Neurophysiol. 97, 3036–3045. https://doi.org/10.1152/jn.01211.2006.

Calderon, C.B., De Loof, E., Ergo, K., Snoeck, A., Boehler, C.N., Verguts, T., 2021. Signed reward prediction errors in the ventral striatum drive episodic memory. J. Neurosci. 41, 1716. https://doi.org/10.1523/JNEUROSCI.1785-20.2020.

Cao, Z., Bennett, M., Orr, C., Icke, I., Banaschewski, T., Barker, G.J., Bokde, A.L.W., Bromberg, U., Büchel, C., Quinlan, E.B., Desrivières, S., Flor, H., Frouin, V., Garavan, H., Gowland, P., Heinz, A., Ittermann, B., Martinot, J.-L., Nees, F., Orfanos, D.P., Paus, T., Poustka, L., Hohmann, S., Fröhner, J.H., Smolka, M.N., Walter, H., Schumann, G., Whelan, R., Consortium, I., 2019. Mapping adolescent reward anticipation, receipt, and prediction error during the monetary incentive delay task. Hum. Brain Mapp. 40, 262–283. https://doi.org/10.1002/hbm.24370.

Clithero, J.A., Smith, D.V., Carter, R.M., Huettel, S.A., 2011. Within- and cross-participant classifiers reveal different neural coding of information. Neuroimage 56, 699–708. https://doi.org/10.1016/j.neuroimage.2010.03.057.

De Loof, E., Ergo, K., Naert, L., Janssens, C., Talsma, D., Van Opstal, F., Verguts, T., 2018. Signed reward prediction errors drive declarative learning. PLoS One 13, e0189212. https://doi.org/10.1371/journal.pone.0189212.

Desikan, R.S., Ségonne, F., Fischl, B., Quinn, B.T., Dickerson, B.C., Blacker, D., Buckner, R.L., Dale, A.M., Maguire, R.P., Hyman, B.T., Albert, M.S., Killiany, R.J., 2006. An automated labeling system for subdividing the human cerebral cortex on MRI scans into gyral based regions of interest. Neuroimage 31, 968–980. https://doi.org/10.1016/j.neuroimage.2006.01.021.

Diederen, K.M.J., Fletcher, P.C., 2020. Dopamine, prediction error and beyond. Neuroscientist 27, 30–46. https://doi.org/10.1177/1073858420907591.

Dolcos, F., Katsumi, Y., Weymar, M., Moore, M., Tsukiura, T., Dolcos, S., 2017. Emerging directions in emotional episodic memory. Front. Psychol. 8, 1867. https://doi.org/10.3389/fpsyg.2017.01867.

Ergo, K., De Loof, E., Verguts, T., 2020. Reward prediction error and declarative memory. Trends Cogn. Sci. 24, 388–397. https://doi.org/10.1016/j.tics.2020.02.009.

Faul, F., Erdfelder, E., Lang, A.-G., Buchner, A., 2007. G*Power 3: a flexible statistical power analysis program for the social, behavioral, and biomedical sciences. Behav Res Methods 39, 175–191. https://doi.org/10.3758/BF03193146.

Fouragnan, E., Retzler, C., Philiastides, M.G., 2018. Separate neural representations of prediction error valence and surprise: Evidence from an fMRI meta-analysis. Hum. Brain Mapp. 39, 2887–2906. https://doi.org/10.1002/hbm.24047.

Frank, L.E., Preston, A.R., Zeithamova, D., 2019. Functional connectivity between memory and reward centers across task and rest track memory sensitivity to reward. Cogn. Affect. Behav. Neurosci. 19, 503–522. https://doi.org/10.3758/s13415-019-00700-8.

Frazier, J.A., Chiu, S., Breeze, J.L., Makris, N., Lange, N., Kennedy, D.N., Herbert, M.R., Bent, E.K., Koneru, V.K., Dieterich, M.E., Hodge, S.M., Rauch, S.L., Grant, P.E., Cohen, B.M., Seidman, L.J., Caviness, V.S., Biederman, J., 2005. Structural brain magnetic resonance imaging of limbic and thalamic volumes in pediatric bipolar disorder. Am. J. Psychiatry 162, 1256–1265. https://doi.org/10.1176/appi.ajp.162.7.1256.

Garrido, M.V., Prada, M., 2017. KDEF-PT: valence, emotional intensity, familiarity and attractiveness ratings of angry, neutral, and happy faces. Front. Psychol. 8, 2181. https://doi.org/10.3389/fpsyg.2017.02181.

Garrison, J., Erdeniz, B., Done, J., 2013. Prediction error in reinforcement learning: a meta-analysis of neuroimaging studies. Neurosci. Biobehav. Rev. 37, 1297–1310. https://doi.org/10.1016/j.neubiorev.2013.03.023.

Gasbarri, A., Packard, M.G., Campana, E., Pacitti, C., 1994. Anterograde and retrograde tracing of projections from the ventral tegmental area to the hippocampal formation in the rat. Brain Res. Bull. 33, 445–452. https://doi.org/10.1016/0361-9230(94)90288-7.

Goldstein, J.M., Seidman, L.J., Makris, N., Ahern, T., O'Brien, L.M., Caviness, V.S., Kennedy, D.N., Faraone, S.V., Tsuang, M.T., 2007. Hypothalamic abnormalities in schizophrenia: sex effects and genetic vulnerability. Biol. Psychiatry 61, 935–945. https://doi.org/10.1016/j.biopsych.2006.06.027.

Hare, T.A., O'Doherty, J., Camerer, C.F., Schultz, W., Rangel, A., 2008. Dissociating the role of the orbitofrontal cortex and the striatum in the computation of goal values and prediction errors. J. Neurosci. 28, 5623–5630. https://doi.org/10.1523/JNEUROSCI.1309-08.2008.

Häusler, A.N., Becker, B., Bartling, M., Weber, B., 2015. Goal or gold: overlapping reward processes in soccer players upon scoring and winning money. PLoS One 10, e0122798. https://doi.org/10.1371/journal.pone.0122798.

Henson, R., 2005. A mini-review of fMRI studies of human medial temporal lobe activity associated with recognition memory. Q. J. Exp. Psychol. B 58, 340–360. https://doi.org/10.1080/02724990444000113.

Jay, T.M., 2003. Dopamine: a potential substrate for synaptic plasticity and memory mechanisms. Prog. Neurobiol. 69, 375–390. https://doi.org/10.1016/S0301-0082(03)00085-6.

Lei, X., Chen, C., Xue, F., He, Q., Chen, C., Liu, Q., Moyzis, R.K., Xue, G., Cao, Z., Li, J., Li, H., Zhu, B., Liu, Y., Hsu, A.S.C., Li, J., Dong, Q., 2014. Fiber connectivity between

the striatum and cortical and subcortical regions is associated with temperaments in Chinese males. Neuroimage 89, 226–234. https://doi.org/10.1016/j.neuroimage.2013.04.043.
Lin, A., Adolphs, R., Rangel, A., 2012. Social and monetary reward learning engage overlapping neural substrates. Soc. Cogn. Affect. Neurosci. 7, 274–281. https://doi.org/10.1093/scan/nsr006.
Lisman, J., Grace, A.A., 2005. The hippocampal-VTA loop: controlling the entry of information into long-term memory. Neuron 46, 703–713. https://doi.org/10.1016/j.neuron.2005.05.002.
Lisman, J., Grace, A.A., Duzel, E., 2011. A neoHebbian framework for episodic memory; role of dopamine-dependent late LTP. Trends Neurosci. 34, 536–547. https://doi.org/10.1016/j.tins.2011.07.006.
Makris, N., Goldstein, J.M., Kennedy, D., Hodge, S.M., Caviness, V.S., Faraone, S.V., Tsuang, M.T., Seidman, L.J., 2006. Decreased volume of left and total anterior insular lobule in schizophrenia. Schizophr. Res. 83, 155–171. https://doi.org/10.1016/j.schres.2005.11.020.
McLaren, D.G., Ries, M.L., Xu, G., Johnson, S.C., 2012. A generalized form of context-dependent psychophysiological interactions (gPPI): a comparison to standard approaches. Neuroimage 61, 1277–1286. https://doi.org/10.1016/j.neuroimage.2012.03.068.
Mumford, J.A., Davis, T., Poldrack, R.A., 2014. The impact of study design on pattern estimation for single-trial multivariate pattern analysis. Neuroimage 103, 130–138. https://doi.org/10.1016/j.neuroimage.2014.09.026.
Mumford, J.A., Turner, B.O., Ashby, F.G., Poldrack, R.A., 2012. Deconvolving BOLD activation in event-related designs for multivoxel pattern classification analyses. Neuroimage 59, 2636–2643. https://doi.org/10.1016/j.neuroimage.2011.08.076.
Murty, V.P., Shermohammed, M., Smith, D.V., Carter, R.M., Huettel, S.A., Adcock, R.A., 2014. Resting state networks distinguish human ventral tegmental area from substantia nigra. Neuroimage 100, 580–589. https://doi.org/10.1016/j.neuroimage.2014.06.047.
Nakashima, S.F., Ukezono, M., Sudo, R., Nunoi, M., Kitagami, S., Okubo, M., Toriyama, R., Morimoto, Y., Takano, Y., 2020. Development of a Japanese version of the 20-item prosopagnosia index (PI20-J) and examination of its reliability and validity. Jpn. J. Psychol. 90, 603–613. https://doi.org/10.4992/jjpsy.90.18235.
Nicholls, M.E.R., Thomas, N.A., Loetscher, T., Grimshaw, G.M., 2013. The flinders handedness survey (FLANDERS): a brief measure of skilled hand preference. Cortex 49, 2914–2926. https://doi.org/10.1016/j.cortex.2013.02.002.
Oikawa, H., Sugiura, M., Sekiguchi, A., Tsukiura, T., Miyauchi, C.M., Hashimoto, T., Takano-Yamamoto, T., Kawashima, R., 2012. Self-face evaluation and self-esteem in young females: an fMRI study using contrast effect. Neuroimage 59, 3668–3676. https://doi.org/10.1016/j.neuroimage.2011.10.098.
Okubo, M., Suzuki, H., Nicholls, M.E., 2014. A Japanese version of the FLANDERS handedness questionnaire. Jpn. J. Psychol. 85, 474–481. https://doi.org/10.4992/jjpsy.85.13235.
Oosterhof, N.N., Todorov, A., 2008. The functional basis of face evaluation. P. Natl. Acad. Sci. USA 105, 11087–11092. https://doi.org/10.1073/pnas.0805664105.
Padoa-Schioppa, C., Cai, X., 2011. The orbitofrontal cortex and the computation of subjective value: consolidated concepts and new perspectives. Ann. N. Y. Acad. Sci. 1239, 130–137. https://doi.org/10.1111/j.1749-6632.2011.06262.x.
Paller, K.A., Wagner, A.D., 2002. Observing the transformation of experience into memory. Trends Cogn. Sci. 6, 93–102. https://doi.org/10.1016/S1364-6613(00)01845-3.
Pine, A., Sadeh, N., Ben-Yakov, A., Dudai, Y., Mendelsohn, A., 2018. Knowledge acquisition is governed by striatal prediction errors. Nat. Commun. 9, 1673. https://doi.org/10.1038/s41467-018-03992-5.
Radloff, L.S., 1977. The CES-D scale: a self-report depression scale for research in the general population. Appl. Psychol. Meas. 1, 385–401. https://doi.org/10.1177/014662167700100306.
Rissman, J., Gazzaley, A., D'Esposito, M., 2004. Measuring functional connectivity during distinct stages of a cognitive task. Neuroimage 23, 752–763. https://doi.org/10.1016/j.neuroimage.2004.06.035.
Samson, Y., Wu, J.J., Friedman, A.H., Davis, J.N., 1990. Catecholaminergic innervation of the hippocampus in the cynomolgus monkey. J. Comp. Neurol. 298, 250–263. https://doi.org/10.1002/cne.902980209.
Schott, B.H., Sellner, D.B., Lauer, C.-J., Habib, R., Frey, J.U., Guderian, S., Heinze, H.-J., Düzel, E., 2004. Activation of midbrain structures by associative novelty and the formation of explicit memory in humans. Learn Memory 11, 383–387. https://doi.org/10.1101/lm.75004.
Schrouff, J., Rosa, M.J., Rondina, J.M., Marquand, A.F., Chu, C., Ashburner, J., Phillips, C., Richiardi, J., Mourão-Miranda, J., 2013. PRoNTo: pattern recognition for neuroimaging toolbox. Neuroinformatics 11, 319–337. https://doi.org/10.1007/s12021-013-9178-1.
Schultz, W., 2016. Dopamine reward prediction error coding. Dialogues Clin. Neurosci. 18, 23–32. https://doi.org/10.31887/DCNS.2016.18.1/wschultz.
Schultz, W., Dayan, P., Montague, P.R., 1997. A neural substrate of prediction and reward. Science 275, 1593–1599. https://doi.org/10.1126/science.275.5306.1593.
Sescousse, G., Caldú, X., Segura, B., Dreher, J.C., 2013. Processing of primary and secondary rewards: a quantitative meta-analysis and review of human functional neuroimaging studies. Neurosci. Biobehav. Rev. 37, 681–696. https://doi.org/10.1016/j.neubiorev.2013.02.002.
Shah, P., Gaule, A., Sowden, S., Bird, G., Cook, R., 2015. The 20-item prosopagnosia index (PI20): a self-report instrument for identifying developmental prosopagnosia. R. Soc. Open Sci. 2 https://doi.org/10.1098/rsos.140343.
Shigemune, Y., Tsukiura, T., Kambara, T., Kawashima, R., 2014. Remembering with gains and losses: effects of monetary reward and punishment on successful encoding activation of source memories. Cereb. Cortex 24, 1319–1331. https://doi.org/10.1093/cercor/bhs415.
Shigemune, Y., Tsukiura, T., Nouchi, R., Kambara, T., Kawashima, R., 2017. Neural mechanisms underlying the reward-related enhancement of motivation when remembering episodic memories with high difficulty. Hum. Brain Mapp. 38, 3428–3443. https://doi.org/10.1002/hbm.23599.
Shima, S., Shikano, T., Kitamura, T., Asai, M., 1985. New self-rating scale for depression. Seisin-Igaku 27, 717–723. https://doi.org/10.11477/mf.1405203967.
Shohamy, D., Adcock, R.A., 2010. Dopamine and adaptive memory. Trends Cogn. Sci. 14, 464–472. https://doi.org/10.1016/j.tics.2010.08.002.
Smith, W.B., Starck, S.R., Roberts, R.W., Schuman, E.M., 2005. Dopaminergic stimulation of local protein synthesis enhances surface expression of GluR1 and synaptic transmission in hippocampal neurons. Neuron 45, 765–779. https://doi.org/10.1016/j.neuron.2005.01.015.
Spaniol, J., Davidson, P.S.R., Kim, A.S.N., Han, H., Moscovitch, M., Grady, C.L., 2009. Event-related fMRI studies of episodic encoding and retrieval: meta-analyses using activation likelihood estimation. Neuropsychologia 47, 1765–1779. https://doi.org/10.1016/j.neuropsychologia.2009.02.028.
Sugar, J., Moser, M.-B., 2019. Episodic memory: neuronal codes for what, where, and when. Hippocampus 29, 1190–1205. https://doi.org/10.1002/hipo.23132.
Sugimoto, H., Dolcos, F., Tsukiura, T., 2021. Memory of my victory and your defeat: contributions of reward- and memory-related regions to the encoding of winning events in competitions with others. Neuropsychologia 152, 107733. https://doi.org/10.1016/j.neuropsychologia.2020.107733.
Tsukiura, T., 2012. Neural mechanisms underlying the effects of face-based affective signals on memory for faces: a tentative model. Front. Integr. Neurosci. 6, 50. https://doi.org/10.3389/fnint.2012.00050.
Tsukiura, T., Cabeza, R., 2008. Orbitofrontal and hippocampal contributions to memory for face–name associations: the rewarding power of a smile. Neuropsychologia 46, 2310–2319. https://doi.org/10.1016/j.neuropsychologia.2008.03.013.
Tsukiura, T., Cabeza, R., 2011a. Remembering beauty: roles of orbitofrontal and hippocampal regions in successful memory encoding of attractive faces. Neuroimage 54, 653–660. https://doi.org/10.1016/j.neuroimage.2010.07.046.
Tsukiura, T., Cabeza, R., 2011b. Shared brain activity for aesthetic and moral judgments: implications for the Beauty-is-Good stereotype. Soc Cogn Affect Neurosci 6, 138–148. https://doi.org/10.1093/scan/nsq025.
Tziortzi, A.C., Searle, G.E., Tzimopoulou, S., Salinas, C., Beaver, J.D., Jenkinson, M., Laruelle, M., Rabiner, E.A., Gunn, R.N., 2011. Imaging dopamine receptors in humans with [11C]-(+)-PHNO: dissection of D3 signal and anatomy. Neuroimage 54, 264–277. https://doi.org/10.1016/j.neuroimage.2010.06.044.
Ueda, R., Yanagisawa, K., Ashida, H., Abe, N., 2018. Executive control and faithfulness: only long-term romantic relationships require prefrontal control. Exp. Brain Res. 236, 821–828. https://doi.org/10.1007/s00221-018-5181-y.
Wakabayashi, A., Tojo, Y., Baron-Cohen, S., Wheelwright, S., 2004. The autism-spectrum quotient (AQ) Japanese version: evidence from high-functioning clinical group and normal adults. Jpn. J. Psychol. 75, 78–84. https://doi.org/10.4992/jjpsy.75.78.
Wake, S.J., Izuma, K., 2017. A common neural code for social and monetary rewards in the human striatum. Soc. Cogn. Affect. Neurosci. 12, 1558–1564. https://doi.org/10.1093/scan/nsx092.
Watabe-Uchida, M., Eshel, N., Uchida, N., 2017. Neural circuitry of reward prediction error. Annu. Rev. Neurosci. 40, 373–394. https://doi.org/10.1146/annurev-neuro-072116-031109.
Wimmer, G.E., Braun, E.K., Daw, N.D., Shohamy, D., 2014. Episodic memory encoding interferes with reward learning and decreases striatal prediction errors. J. Neurosci. 34, 14901–14912. https://doi.org/10.1523/JNEUROSCI.0204-14.2014.
Wittmann, B.C., Schott, B.H., Guderian, S., Frey, J.U., Heinze, H.-J., Düzel, E., 2005. Reward-related fMRI activation of dopaminergic midbrain is associated with enhanced hippocampus- dependent long-term memory formation. Neuron 45, 459–467. https://doi.org/10.1016/j.neuron.2005.01.010.
Yarkoni, T., Poldrack, R.A., Nichols, T.E., Van Essen, D.C., Wager, T.D., 2011. Large-scale automated synthesis of human functional neuroimaging data. Nat. Methods 8, 665–670. https://doi.org/10.1038/nmeth.1635.
Zaghloul, K.A., Blanco, J.A., Weidemann, C.T., McGill, K., Jaggi, J.L., Baltuch, G.H., Kahana, M.J., 2009. Human substantia nigra neurons encode unexpected financial rewards. Science 323, 1496–1499. https://doi.org/10.1126/science.1167342.